Retinal Analog Study of the Role of Steric Interactions in the Excited State Isomerization Dynamics of Rhodopsin†

Gerd G. Kochendoerfer,‡ Peter J. E. Verdegem,§ Ineke van der Hoef,§ Johan Lugtenburg,§ and Richard A. Mathies*,‡

Department of Chemistry, University of California, Berkeley, California 94720, and Leiden Institute of Chemistry, University of Leiden, 2300 RA Leiden, The Netherlands

Received August 6, 1996; Revised Manuscript Received October 21, 1996⊗

ABSTRACT: The role of intramolecular steric interactions in the isomerization of the 11-*cis*-retinal chromophore in the photoreceptor protein rhodopsin is examined with resonance Raman and CD spectroscopy combined with quantum yield experiments. The resonance Raman spectra and CD spectra of 13-demethylrhodopsin indicate that its chromophore, an analog in which the nonbonded interaction between the 10-H and the 13-CH_3 groups is removed, is less distorted in the $C_{10}\cdots C_{13}$ region than the native chromophore. The reduced torsional and hydrogen-out-of-plane resonance Raman intensities further indicate that the excited state potential energy surface has a much shallower slope along the isomerization coordinate. This is consistent with the decrease in quantum yield from 0.67 in rhodopsin to 0.47 in 13-demethylrhodopsin. The resonance Raman intensities show that the steric twist is reintroduced by addition of a methyl group at the C_{10} position. However, the quantum yield of 10-methyl-13-demethylrhodopsin is found to be only 0.35. This is attributed to nonisomorphous protein−analog interactions. The nonbonded interaction between the 10-hydrogen and the 13-methyl group in 11-*cis*-retinal makes this isomer particularly effective as the light-sensing chromophore in all visual pigments.

The primary event in vision is the ultrafast *cis*−*trans* isomerization of the 11-*cis*-retinal chromophore in the photoreceptor protein rhodopsin. This efficient ($\Phi = 0.67$) isomerization initiates a sequence of protein conformational changes that trigger a nerve impulse (Stryer, 1991; Yoshizawa & Wald, 1967). Recent femtosecond time-resolved transient absorption experiments have demonstrated that the primary photoproduct of rhodopsin is formed in only 200 fs (Peteanu et al., 1993; Schoenlein et al., 1991). This rapid formation time led to the hypothesis that the high reaction efficiency is mechanistically linked to the rapid isomerization rate through a Landau−Zener type dynamic internal conversion process (Landau, 1932; Zener, 1932). This hypothesis has found additional support through the recent observation of coherent vibrational oscillations in the photoproduct following impulsive excitation of the reactant (Wang et al., 1994). It was further hypothesized that the rapid isomerization rate is driven by the nonbonded interaction between the 13-CH_3 group and the 10-H in the 11-*cis*-retinal chromophore (see Figure 1). This interaction introduces a torsional distortion of the chromophore in the $C_{10}\cdots C_{13}$ region (Eyring et al., 1982) and is expected to introduce a significant slope in the Franck−Condon region of the excited state surface along the $C_{11}{=}C_{12}$ torsional coordinate. Upon excitation, the chromophore is expected to rapidly accelerate out of the Franck−Condon region along this coordinate, leading to very efficient dynamic coupling between the excited state of the reactant and the ground state of the photoproduct.

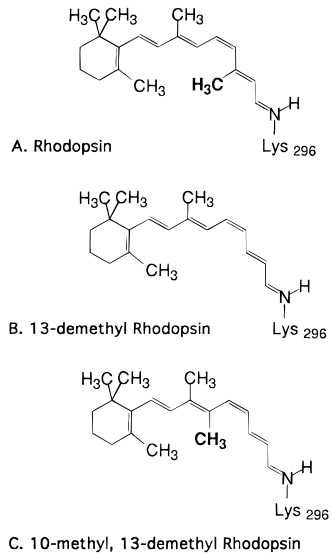

FIGURE 1: Chromophore structures of rhodopsin, 13-demethylrhodopsin, and 10-methyl-13-demethylrhodopsin.

This hypothesis about the role of nonbonded interactions in the isomerization process was first tested in studies of isorhodopsin, a 9-*cis*-retinal rhodopsin analog whose different chromophore geometry eliminates the steric interaction between the 13-CH_3 and the 10-H groups. The slower photoproduct formation rate of 600 fs correlates well with the reduced reaction quantum yield of 0.22 (Hurley et al., 1977), supporting our hypothesis (Schoenlein et al., 1993). Recent experiments demonstrating that the fluorescence lifetime of isorhodopsin is twice as long as that of rhodopsin show that the initial torsional dynamics in the Franck−Condon region for this analog are significantly slower

† This work was supported by NIH Grant EY-02051 (R.A.M.). P.J.E.V. acknowledges generous support from the European Community Biotechnology Program CEC Project PL 92-0467.

* Author to whom correspondence should be addressed.
‡ University of California.
§ University of Leiden.

⊗ Abstract published in *Advance ACS Abstracts,* December 1, 1996.

S0006-2960(96)01951-4 CCC: $12.00

(Kochendoerfer & Mathies, 1996). However, we were interested in testing our hypothesis on a retinal analog that is structurally more similar to 11-*cis*-retinal. The most direct approach is to study 13-demethylrhodopsin, an 11-*cis*-retinal analog in which the 13-CH_3 group has been replaced by a hydrogen. Recent femtosecond time-resolved absorption experiments have demonstrated that the photoproduct formation time for this analog is slowed to 400 fs (Wang et al., 1996). To fully understand and interpret this result, we characterize the structural and photophysical properties of this analog in more detail.

In this paper, we further investigate the role of nonbonded interactions in the torsional dynamics and isomerization mechanism of 11-*cis*-retinal pigments by performing quantum yield as well as resonance Raman and CD[1] spectroscopic measurements on rhodopsin analogs regenerated with 13-demethyl- and 10-methyl-13-demethylretinal. The Raman intensities indicate that removal of the 13-CH_3 group eliminates the torsional deformation of the chromophore as well as the steep slope of the excited state potential surface along the C_{11}=C_{12} isomerization coordinate. The reaction quantum yield decreases to 0.47 upon removal of the steric interaction in 13-demethylrhodopsin, but contrary to simple expectation, the quantum yield decreases further to 0.35 in 10-methyl-13-demethylrhodopsin. The inability of this pigment to recover the high reaction efficiency of rhodopsin appears to be due to unfavorable interactions between the analog chromophore and its protein environment.

EXPERIMENTAL PROCEDURES

Sample Preparation. The synthesis of 13-demethylretinal was accomplished by a Horner−Wadsworth−Emmonds (HWE) coupling of 3-cyano-2-propenyl diethylphosphonate with *all-trans*-β-ionylidene acetaldehyde and subsequent reduction of the nitrile function with Dibal-H. Purification of the *all-trans* isomer was accomplished by silica gel chromatography (eluent was 20:80 diethyl ether/petroleum ether). The spectroscopic characteristics of *all-trans*-13-demethyl retinal are in agreement with the literature (Broek et al., 1983). 11-*cis*-13-Demethylretinal was prepared by photoisomerization of the *all-trans* isomer as described before (Broek et al., 1983). For the synthesis of 10-methyl-13-demethylretinal, β-ionone was coupled with 1-(1-cyanoethyl) diethylphosphonate in a HWE coupling and the nitrile function was subsequently reduced with Dibal-H, resulting in 2-(β-ionylidene)propanal. Elongation of the conjugated chain was achieved by a HWE coupling of the aldehyde with 3-(1-cyano-2-methylpropenyl) diethylphosphonate and subsequent reduction with Dibal-H, resulting in 10-methyl-13-demethylretinal. The *all-trans* isomer was purified by silica gel chromatography (eluent was 20:80 diethyl ether/petroleum ether). The purity of *all-trans*-10-methyl-13-demethylretinal was confirmed by ^{1}H-NMR. The 11-*cis*-10-methyl-13-demethylretinal was prepared by photoisomerization of the *all-trans* isomer following methods used for 13-demethylretinal (Broek et al., 1983). 11-*cis*-Retinal was a generous gift from Rosalie Crouch.

The protonated Schiff base (PSB) of 10-methyl-13-demethylretinal was synthesized by adding a 20-fold excess of *n*-butylamine to 1 mL of a solution containing 300 μg of retinal in hexane (Palings et al., 1987). The solution was allowed to react for 30 min at room temperature to form the retinal Schiff base. The solvent was evaporated under a stream of N_2 gas and the residue dissolved in ~400 μL of dried methanol. The solution was titrated with aliquots of acidified methanol (~200 μL of 12 M HCl dissolved in 5 mL of dry methanol) until no further increase in absorbance at 440 nm was detected.

Rod outer segments (ROS) were isolated from 200 bovine retinas (J. A. Lawson, Lincoln, NE) by sucrose flotation followed by sucrose density gradient centrifugation as described previously (Applebury et al., 1974; Palings et al., 1987). The ROS were bleached in the presence of 20 mM NH_2OH and washed with 20 mM PIPES [piperazine-*N*,*N*′-bis(2-ethanesulfonic acid)] three times to remove excess NH_2OH. The resulting opsin suspension was dissolved in 20 mM CHAPSO buffer and mixed with a 3-fold excess of retinal analog for 4−15 h. The regeneration of the pigment was followed by monitoring the absorbance at 500 nm. After no further increase was detected, the regeneration mixture was applied to a concanavalin A-Sepharose 4B affinity column that had been equilibrated with 20 mM PIPES (pH 6.5) supplemented with buffer A [20 mM CHAPSO, 150 mM NaCl, 1 mM $CaCl_2$, 1 mM $MgCl_2$, 1 mM $MnCl_2$, and 0.1 mM EDTA (De Grip, 1982)]. The column was thoroughly washed until the eluent did not show any residual absorption at 380 nm due to excess retinal and retinal oxime. The pigment was eluted with buffer A supplemented with 200 mM α-methyl mannoside. To obtain the rhodopsin samples used as a quantum counter in the quantum yield experiments, the ROS were dissolved in buffer A and directly applied to the concanavalin A-Sepharose 4B affinity column as described above. The 10-methyl-13-demethylrhodopsin sample in D_2O was obtained by dialysis of the elutant into deuterated buffer A using dialysis cassettes (Slide-A-Lyzer, Pierce, Rockford, IL).

Raman Spectroscopy. Room-temperature, rapid-flow resonance Raman spectra of the rhodopsin analogs in buffer A + 50 mM α-methyl mannoside were obtained with 10 mL samples having an absorbance of 0.3−1.0 OD/cm at 500 nm. Resonance Raman scattering was excited by spherically focusing (focal length of 75 mm) the 530.9 nm output of a Kr^+ laser in the 600 μm diameter capillary containing the flowing pigment solution. The laser power (160 μW), flow rate (300 cm/s), and beam waist (15 μm) were chosen to minimize the effects of photolysis on the Raman spectra (photoalteration of <0.1; Mathies et al., 1976). Preresonance Raman spectra of the 11-*cis*-10-methyl-13-demethyl PSB were obtained by spherically focusing (focal length of 75 mm) the 752.0 nm output of a Kr^+ laser (15 mW) on a 1 mm diameter capillary containing the PSB in MeOH. Detection was accomplished with a cooled CCD detector (Princeton Instruments, LN1152) coupled to a Spex 1401 double spectrograph. Spectral slit widths were 5 cm^{-1}. The spectrometer was calibrated with cyclohexanone as an external standard. Frequencies are accurate to ±1 cm^{-1}. Each spectrum was divided by a tungsten halogen lamp spectrum (Eppley Laboratories Inc., Newport, RI) to correct for the spectrometer response and detection sensitivity.

Photosensitivity Experiments. The isomerization quantum yield of the pigment analogs was determined by measuring the initial photobleaching rate of the analog pigments and native rhodopsin at a single wavelength (Liu et al., 1986).

[1] Abbreviations: CD, circular dichroism; HWE, Horner−Wadsworth−Emmonds; CHAPSO, 3-[[(3-cholamidopropyl)dimethyl]ammonio]-2-hydroxy-1-propane sulfonate; PSB, protonated Schiff base; PIPES, piperazine-*N*,*N*′-bis(2-ethanesulfonic acid); HOOP, hydrogen-out-of-plane.

The photochemical decay is described by the rate law

$$\frac{dc(t)}{dt} = -I\Phi \tag{1}$$

where $c(t)$ is the molar concentration of the reactant, I is the number of photons absorbed per time and volume, and Φ is the reaction quantum yield. For low-optical density solutions, the number of photons absorbed is given by Beer's law as

$$I = I_0 \times 2.3\epsilon l c(t) \tag{2}$$

where ϵ is the molar extinction coefficient, l is the path length of the sample, and I_0 is the initial light intensity. Substituting eq 2 into eq 1 followed by integration yields the equation for the initial bleaching kinetics:

$$c(t) = c(0) - 2.3I_0A(0)\Phi t \tag{3}$$

where $A(0)$ is the absorbance of the sample at $t = 0$. Since we measure the decay rate of the absorbance, the final equation relating the absorbance to the quantum yield is

$$A(t) = A(0)(1 - 2.3lI_0\Phi\epsilon t) \tag{4}$$

If the photoproduct does not absorb at the probing wavelength, one expects a linear initial decrease of absorption with time with a slope of $2.3lI_0A(0)\Phi\epsilon$. The extinction coefficient ϵ is determined in a separate experiment (see below). Since I_0 is quite difficult to measure independently, the reaction quantum yield of the analogs is determined by using rhodopsin as a quantum counter. We determine the ratio ρ of the respective decay rates of the analog proteins and rhodopsin. The intensity I_0 is thereby eliminated, and the results are referenced to the experimentally well-established quantum yield and extinction coefficient of rhodopsin (Dartnall et al., 1936; Gaertner et al., 1991; Wald & Brown, 1954).

$$\Phi^{\text{analog}} = \Phi^{\text{rho}}\rho\frac{[A(0)^{\text{rho}}\epsilon^{\text{rho}}]}{[A(0)^{\text{analog}}\epsilon^{\text{analog}}]} \tag{5}$$

While all samples were prepared and stored in buffer A, the photobleaching experiments were performed in Ammonyx-LO to ensure complete sample bleaching (see below). Prior to the experiment, aliquots of pigment stock solutions in buffer A (0.3−1 OD/cm at 500 nm) were diluted with 3% Ammonyx buffer (30 mM HPO_4^{2-}) to 0.03−0.1 OD/cm at λ_{max}. In each experiment, 3.5 mL of either the dilute rhodopsin or the analog pigment solution and a buffer blank were placed into a DW2 absorption spectrometer (SLM Aminco, Urbana, IL) and cooled to 10 °C. A stream of nitrogen was blown over both faces of the cuvettes to prevent fogging. The instrument was set to kinetic mode, and the decay of absorbance was measured at 500 and 530 nm. The light beam used to measure the absorption was used as the actinic beam as well. The long term stability of the spectrometer lamp was rated greater than 0.1%. The sample was mechanically stirred to ensure homogeneous bleaching of the entire solution. Due to the different thermal stability of the pigment analogs relative to that of rhodopsin, we also had to control for spontaneous sample decay by measuring a "background bleaching rate". This rate was determined by setting the illumination bandwidth to 2 nm and monitoring the absorption decay for 20 min. The illumination bandwidth was then increased to 12 nm and the decay of absorbance followed for 20 min. The difference in the absorption decay rate between these two measurements is a direct measurement of the photochemical bleaching due to the additional photons at the higher bandwidth. Experiments were performed measuring both the decay at 500 and 530 nm, and the results agreed within experimental error. The decay at low bandwidths and high bandwidths for each pigment were analyzed by linear regression. Subtracting the low-bandwidth decay rate from the high-bandwidth rate yielded the purely photochemical bleaching rate.

Determination of the Extinction Coefficient. The most common method for determining the extinction coefficient is bleaching the pigment in the presence of NH_2OH and comparing the retinal oxime absorption to the original pigment absorption (Gaertner et al., 1991; Nelson et al., 1970). Another method is to concurrently regenerate identical opsin solutions with 11-*cis*-retinal and retinal analog and to compare the resulting absorption spectra (Liu et al., 1986). While the first approach can lead to erroneous results due to the large fluctuation of the extinction coefficient of retinal oxime in a complex mixture of membrane and detergent, the second approach can be imprecise if there is incomplete regeneration of opsin with the retinal analog.

Our new approach is based on the observation that the chromophore of 13-demethylrhodopsin can be exchanged for 11-*cis*-retinal (Nelson et al., 1970). Measuring the change in absorbance upon conversion of the analog pigment to wild-type rhodopsin can be used to determine the relative extinction coefficient of the analogs. The following assay is used to probe the extent of chromophore exchange. While wild-type rhodopsin is stable in the presence of 50 mM NH_2OH, 13-demethylrhodopsin (Nelson et al., 1970) and 10-methyl-13-demethylrhodopsin are bleached by NH_2OH in the dark. When the pigment solutions are incubated with 50 mM NH_2OH, the nonexchanged analog protein bleaches, while the newly formed wild-type rhodopsin is stable. The fraction of absorbance remaining after prolonged incubation with NH_2OH reflects the extent of chromophore replacement.

A 3−10-fold excess of 11-*cis*-retinal was mixed with 10 mL of pigment analog solution (buffer A, 20 mM mannose, 1% DTT, and optical density of ∼0.1 OD/cm at 500 nm). The samples were stirred at 12 °C, and 1 mL aliquots were removed after 10 min and 24 h. Control experiments showed that the rhodopsin analogs were stable under these experimental conditions for more than 24 h. Absorption spectra were taken of each aliquot. Then, 50 μL of 1 M NH_2OH (pH 7) was added to each aliquot, and the absorption spectrum was taken after ∼24 h of incubation at 8 °C.

The extinction coefficients of the pigments were found to be dependent on their detergent environment. The experiment described above measures the relative extinction coefficient in buffer A. The ratio of the extinction coefficients of the pigments in buffer A and Ammonyx/HPO_4^{2-} used in our quantum yield experiments was obtained by adding a 5-fold excess of buffer A or Ammonyx/HPO_4^{2-}, respectively, to a small volume of pigment solution in buffer A and comparing the change in absorbance between the two detergent systems.

Computational Methods. The geometry and normal modes of 11-*cis*-retinal PSB, 11-*cis*-13-demethyl PSB, and 11-*cis*-10-methyl-13-demethyl PSB were calculated using the QCFF-PI method (Palings et al., 1987; Warshel, 1973). The

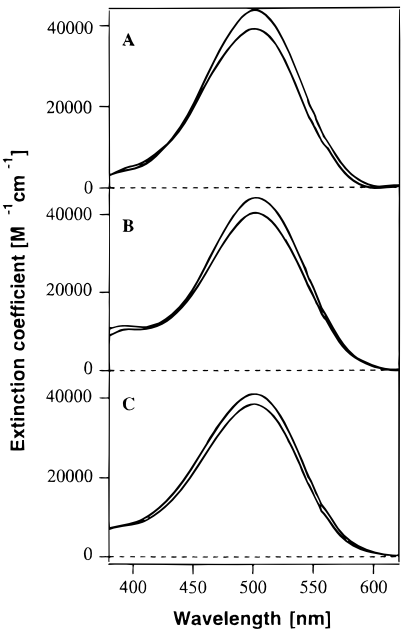

FIGURE 2: Visible absorption spectra of rhodopsin (A), 13-demethylrhodopsin (B), and 10-methyl-13-demethylrhodopsin (C). For all three proteins, the lower curve gives the absolute absorption spectrum in CHAPSO (buffer A) and the upper curve is in 3% Ammonyx (30 mM HPO_4^{2-}).

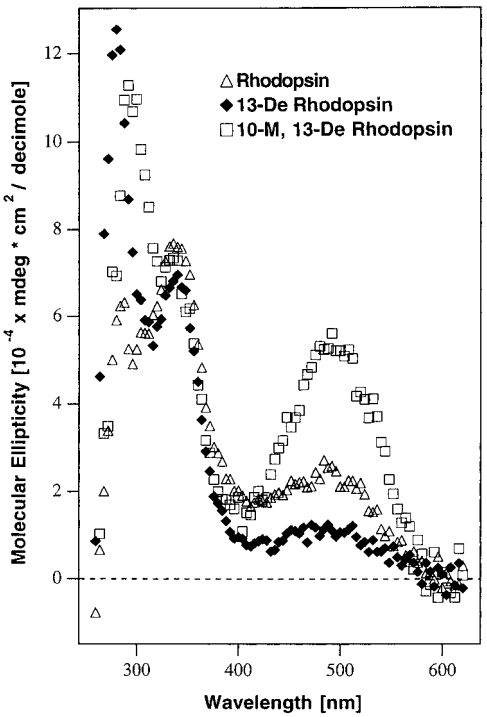

FIGURE 3: CD spectra of rhodopsin (△), 13-demethyl rhododopsin (◆), and 10-methyl-13-demethylrhodopsin (□). All three pigment samples were purified on a concanavalin A column and eluted in buffer A (200 mM α-methylmannose). A background CD spectrum of the elution buffer has been subtracted. The sample absorbance was 0.4 OD/cm at 500 nm. Absorption spectra taken before and after the CD measurement indicated that the protein absorbance decreased by less than 5% during a measurement. Spectra were obtained on a Jasco J-600 spectropolarimeter.

chromophore was truncated by replacing the δ-carbon of the lysine group with a group that has a mass of 15, a valence of 1, and the potential parameters of an sp^3 carbon.

RESULTS

Figure 2 demonstrates that opsin regenerates with 11-*cis*-13-demethylretinal to form a pigment with an absorption maximum at 498 nm, in good agreement with previously published results (Lin, 1994; Nelson et al., 1970; Randall et al., 1991). 11-*cis*-10-Methyl-13-demethylretinal regenerates to form a pigment with an absorption maximum at 500 nm. These absorption maxima and spectral bandwidths are very similar to those of rhodopsin (λ_{max} = 500 nm). The absorption spectra of the pigments in Ammonyx/HPO_4^{2-} and buffer A were determined, and the relative extinctions in these two buffer systems are also indicated. In all cases, the upper curve is for Ammonyx and the lower curve is for CHAPSO.

The CD spectra of rhodopsin, 13-demethylrhodopsin, and 10-methyl-13-demethylrhodopsin are displayed in Figure 3. The CD spectrum of rhodopsin has two bands in the visible region at ~490 and ~340 nm, consistent with previously published results (Honig et al., 1973; Rafferty et al., 1977; Yoshizawa & Shichida, 1982). The CD spectrum of 13-demethylrhodopsin is consistent with the previously published spectrum (Nelson et al., 1970). It exhibits one band at ~490 nm with much less intensity than that of rhodopsin and one at ~340 nm with an intensity similar to that of rhodopsin. An additional large band is found at 280 nm. The CD spectrum of 10-methyl-13-demethylrhodopsin exhibits a band at ~490 nm that is more than twice as large as that of rhodopsin. The band at 340 nm is very similar to that of rhodopsin.

Raman Spectroscopy. The resonance Raman spectra of rhodopsin, 13-demethylrhodopsin, 10-methyl-13-demethylrhodopsin, and the 11-*cis*-10-methyl-13-demethyl PSB are presented in Figure 4. The resonance Raman spectrum of rhodopsin has been extensively studied previously (Mathies et al., 1987; Palings et al., 1987, 1989). Our spectrum is in excellent agreement with previously published spectra. Briefly, the intense mode at 973 cm^{-1} is the HC_{11}═$C_{12}H$ A_2 hydrogen-out-of-plane (HOOP) mode. The modes between 1191 and 1268 cm^{-1} are single-bond stretches and hydrogen-in-plane rocks, and the mode at 1549 cm^{-1} is the ethylenic stretching mode. The mode at 1655 cm^{-1} is the C═NH^+ stretching mode. The band at 569 cm^{-1}, which is more clearly displayed in Figure 5, has very recently been assigned to the C_{11}═C_{12} torsional motion (Lin, 1994).

The Raman spectra of 13-demethylrhodopsin and 10-methyl-13-demethylrhodopsin are presented in panels B and C of Figure 4. The main features of the 13-demethyl spectrum are reduced intensity HOOP modes at 975 and 989 cm^{-1}, two prominent fingerprint modes at 1185 and 1248 cm^{-1}, the ethylenic stretching vibration at 1549 cm^{-1}, and the C═NH^+ stretching vibration at 1662 cm^{-1}. The main features of the 10-methyl-13-demethyl spectrum are the reappearance of strong intensity in the HOOP modes at 967 and 989 cm^{-1}, fingerprint modes at 1195, 1247, and 1302 cm^{-1}, the ethylenic stretching vibration at 1538 cm^{-1}, and the C═NH^+ stretching vibration at 1669 cm^{-1}. The C═NH^+ stretching mode of this analog shifts to 1631 cm^{-1} upon deuteration (Figure 4D). This frequency reduction is caused by the uncoupling of the NH rocking mode from the C═NH^+ stretching mode, and the magnitude of the downshift is an indication of the strength of hydrogen bonding of the Schiff base group (Baasov et al., 1987). The 38 cm^{-1} downshift observed in 10-methyl-13-demethylrhodopsin is indicative of very strong hydrogen bonding in this analog. In rhodopsin, in which hydrogen bonding of the PSB hydrogen is

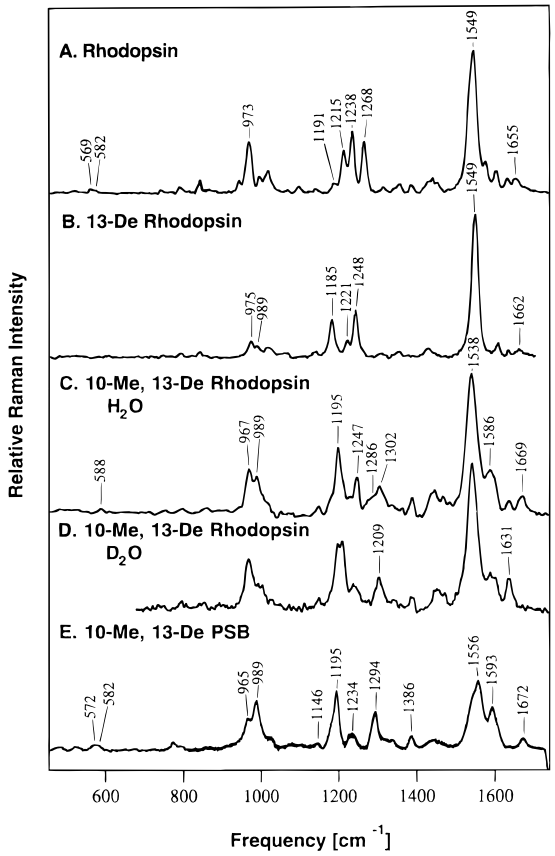

FIGURE 4: Rapid-flow resonance Raman spectra of rhodopsin (A), 13-demethylrhodopsin in H_2O (Lin, 1994) (B), and 10-methyl-13-demethylrhodopsin in H_2O (C) and D_2O (D) and preresonance Raman spectrum of 10-methyl-13-demethylretinal protonated Schiff base in methanol (E). The rhodopsin spectra (A, C, and D) were obtained with 600 μW of 514.5 nm excitation. The protonated Schiff base spectrum was obtained with 15 mW of 752 nm excitation.

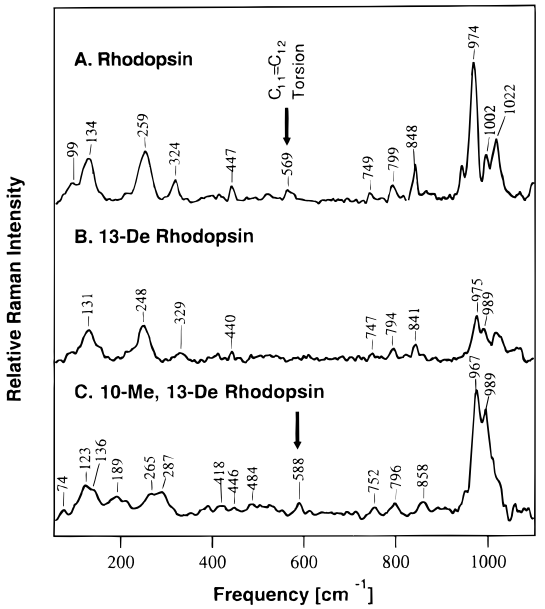

FIGURE 5: Low-frequency region of the rapid-flow resonance Raman spectra of rhodopsin (A), 13-demethylrhodopsin in H_2O (B) (Lin, 1994), and 10-methyl-13-demethylrhodopsin in H_2O (C). The rhodopsin spectra (A and C) were obtained with 600 μW of 514.5 nm excitation. The spectra were normalized to give identical intensity in the ethylenic resonance Raman line. The C_{11}=C_{12} torsional band is indicated by the arrow.

believed to be strong, the C=NH^+ stretch decreases by 31 cm^{-1} (Deng et al., 1994; Mathies et al., 1987; Oseroff & Callender, 1974).

Fingerprint Modes. The fingerprint modes of 13-demethylrhodopsin and 10-methyl-13-demethylrhodopsin are assigned by comparison with the fingerprint spectrum of rhodopsin. The expected changes in the vibrational spectra of the retinal analogs are discussed in more detail, and a correlation diagram of the fingerprint and HOOP modes of rhodopsin and the two analogs will be found in the Supporting Information. In 13-demethylrhodopsin, we expect a large downshift of the $C_{12}-C_{13}$ stretching mode from 1238 cm^{-1} in rhodopsin due to removal of the coupling of this mode with the 13-CH_3 stretch. We therefore assign the mode at 1185 cm^{-1} in 13-demethylrhodopsin to a mixed $C_{10}-C_{11}$, $C_{12}-C_{13}$, and $C_{14}-C_{15}$ stretching vibration. The remaining modes at 1221 and 1248 cm^{-1} are assigned to the C_8-C_9 stretch (since this mode is expected to change little from that of rhodopsin) and to the HC_{11}=C_{12}H A_1 rock, respectively. QCFF-PI calculations predict the HC_{11}=C_{12}H A_1 rocking band at this lower frequency (1244 cm^{-1}) relative to rhodopsin, possibly due to the reduced coupling with the $C_{12}-C_{13}$ stretching mode.

For 10-methyl-13-demethylrhodopsin, we assign the modes at 1302 cm^{-1} to a combination of C_8-C_9 and $C_{10}-C_{11}$ stretching vibrations. The latter is expected to shift up by $\sim$100 cm^{-1} due to methyl substitution, allowing for mixing with higher-frequency modes. QCFF-PI calculations predict that the mode is a mixture of C_8-C_9 and $C_{10}-C_{11}$ stretching vibrations and the HC_{11}=C_{12}H A_1 rocking vibration. The band at 1247 cm^{-1} is predicted to be the HC_{11}=C_{12}H A_1 rocking vibration mixed with the $C_{10}-C_{11}$ stretch. The band at 1195 cm^{-1} is assigned by comparison with the QCFF-PI prediction to a combination of $C_{12}-C_{13}$ and $C_{14}-C_{15}$ stretches coupled to the neighboring rocks.

HOOP Modes. The pattern of modes in the HOOP region of 13-demethylrhodopsin and 10-methyl-13-demethylrhodopsin is governed by the characteristic vibrational frequencies and couplings of the individual hydrogen wags. The expected changes in the vibrational spectra of the retinal analogs are discussed in more detail in the Supporting Information. In polyenes, hydrogen wags couple across double bonds to form in-phase and out-of-phase HOOP combinations. However, wags that are separated by a substituted ethylenic carbon do not interact strongly with each other. The removal of the 13-methyl group allows the HC_{11}=C_{12}H A_2, the HC_{13}=C_{14}H A_u HOOP, and the $C_{15}-H$ wag vibrations to couple across the neighboring single bonds. While unperturbed symmetric HOOP vibrations are expected to appear around 970 cm^{-1}, the coupling of two HOOP modes is expected to result in a splitting between those modes by $\sim$20 cm^{-1}, yielding bands at around 950 and 990 cm^{-1}. Normal mode calculations using both the modified Urey−Bradley force field and the QCFF-PI force field yield very similar predictions, suggesting that the observed coupling patterns are mainly governed by the local molecular geometry and less by the specific bond force constants employed (Curry, 1983). This coupling pattern is also observed in a number of small molecules, including retinals, as discussed in the Supporting Information.

The Raman spectrum of 13-demethylrhodopsin displays two HOOP modes: a medium weak line at 975 cm^{-1} and a weak line at 989 cm^{-1}. The line at 975 cm^{-1} is assigned to the HC_7=C_8H A_u HOOP vibration and the line at 989 cm^{-1} to the higher frequency combination of the HC_{11}=C_{12}H A_2 HOOP and HC_{13}=C_{14}H A_u HOOP vibrations. The frequency

of the line at 975 cm^{-1} is too high to be assigned to the low-frequency combination of the $HC_{11}=C_{12}H$ A_2 HOOP and $HC_{13}=C_{14}H$ A_u HOOP vibrations.[2]

The frequencies of the HOOP modes of 10-methyl-13-demethylrhodopsin have a pattern similar to that of the HOOP region of 13-demethylrhodopsin, but their intensities are much higher. We therefore assign the mode at 967 cm^{-1} to the $HC_7=C_8H$ A_u HOOP vibration and the mode at 989 cm^{-1} to the high-frequency combination of the $HC_{11}=C_{12}H$ A_2 HOOP and $HC_{13}=C_{14}H$ A_u HOOP vibrations. The lower frequency of the $HC_7=C_8H$ A_u HOOP vibration compared to that of 13-demethylrhodopsin is possibly due to the absence of coupling of this mode with the 10-H wag in this case. A similar behavior is found in isorhodopsin, where deuteration of the 10-H leads to a frequency decrease of the $HC_7=C_8H$ A_u HOOP mode by 7 cm^{-1} (Eyring et al., 1982). The mode at 989 cm^{-1} loses intensity in D_2O, while the mode at 967 cm^{-1} does not show any changes, suggesting that the 967 cm^{-1} mode is more isolated and remote from the Schiff base terminus (Figure 4D).

The assignments of the HOOP modes are consistent with QCFF-PI calculations on the protonated Schiff base of 10-methyl-13-demethylretinal. The calculations predict a HOOP mode made up of $HC_{11}=C_{12}H$ and $C_{15}H$ wagging at 990 cm^{-1}, the $HC_7=C_8H$ A_u HOOP mode at 971 cm^{-1}, and an additional HOOP mode at 956 cm^{-1} made up of $HC_{13}=C_{14}H$ and $C_{15}H$ wagging. The HOOP mode at 990 cm^{-1} is predicted to decrease in intensity and downshift by 4 cm^{-1} upon deuteration which is consistent with the experimental results. In the Supporting Information, the results of the QCFF-PI calculations on the wagging vibrations are presented in Table 2 and a correlation diagram is presented in Figure 9.

Low-Frequency Modes. Significant differences between rhodopsin and the two analog proteins are also observed in the low-frequency region of the Raman spectra displayed in Figure 5. The rhodopsin mode at 569 cm^{-1} has been assigned to the torsion around $C_{11}=C_{12}$ (Lin, 1994). No mode of similar intensity is observed in the double-bond torsional region of the Raman spectrum of 13-demethylrhodopsin. This is consistent with the idea that the steric interaction between the 10-H and the 13-CH_3 group has been removed and the $C_{11}=C_{12}$ torsional distortion relaxed. The resonance Raman spectrum of 10-methyl-13-demethylrhodopsin has a band at 588 cm^{-1} in the double-bond torsional region. The QCFF-PI calculations predict two modes around 588 cm^{-1} composed of the 9-CH_3 and 10-CH_3 wags and significant contribution from the C_8-C_9 and $C_{11}=C_{12}$ torsions. In addition, the calculations predict a mode at 473 cm^{-1} with the main contribution from the $C_{11}=C_{12}$ torsion. The calculations indicate that upon adding the 10-CH_3 group the intensity of the modes with $C_{11}=C_{12}$ torsional character increases. We therefore assign the 588 cm^{-1} mode in 10-methyl-13-demethylrhodopsin to the $C_{11}=C_{12}$ torsion that has gained intensity due to out-of-plane distortion of the chromophore caused by reintroduction of nonbonded interaction. The result of the QCFF-PI calculations on the torsional modes is provided in Table 3 of the Supporting Information.

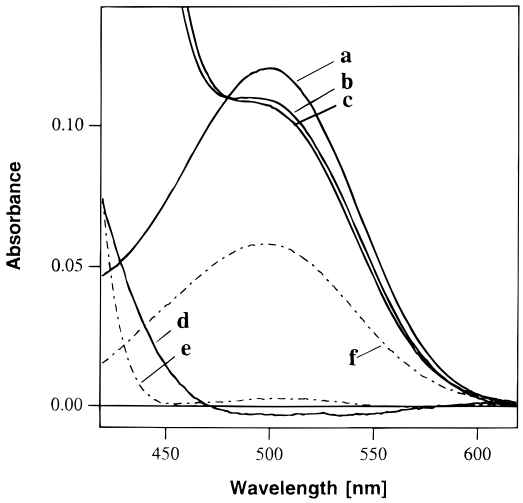

FIGURE 6: Absorption spectrum of 10-methyl-13-demethylrhodopsin (a) and absorption spectra of the same solution after mixing with 11-*cis*-retinal for 10 min (b) and 24 h (c). The difference between the solutions after 24 h of incubation and after 10 min of incubation is displayed in trace d (=c − b). The dashed traces present the spectra of the samples incubated with retinal for 10 min (trace e) and 24 h (trace f) followed by treatment with NH_2-OH to determine the amount of analog pigment present.

11-cis-10-Methyl-13-*demethylretinal PSB.* The preresonance Raman spectrum of the PSB presented in Figure 4E is assigned by comparison to the Raman spectrum of 10-methyl-13-demethylrhodopsin. The $C=NH^+$ stretching frequency is assigned at 1672 cm^{-1}, very close to its value in 10-methyl-13-demethylrhodopsin. The ethylenic region exhibits lines with maxima at 1556 and 1593 cm^{-1}. The mode at 1294 cm^{-1} is assigned to the mixed C_8-C_9 and $C_{10}-C_{11}$ stretches and the mode at 1195 cm^{-1} to a combination of the mixed $C_{10}-C_{11}$, $C_{12}-C_{13}$, and $C_{14}-C_{15}$ stretching vibrations. The broad band at 1234 cm^{-1} is assigned to the $HC_{11}=C_{12}H$ A_1 rocking vibration and the $C_{10}-C_{11}$ stretch. We assign the mode at 965 cm^{-1} to the $HC_7=C_8H$ A_u HOOP vibration and the mode at 989 cm^{-1} to the coupled $HC_{11}=C_{12}H$ A_2 HOOP and $HC_{13}=C_{14}H$ A_u HOOP vibrations.

Extinction Coefficient Determination. Figure 6 presents the absorption spectrum of 10-methyl-13-demethylrhodopsin prior to addition of 11-*cis*-retinal (trace a) and the spectrum of the same sample 10 min (trace b) and 24 h (trace c) after addition of a 10-fold excess of 11-*cis*-retinal. After 10 min of incubation, only a small fraction of the chromophores have been exchanged. In a control experiment, we determined that opsin regenerates with 11-*cis*-retinal with a half-time of 5 min under our experimental conditions. The absence of any significant increase in absorbance at 500 nm after 10 min shows that there is no significant amount of regeneratable opsin in our purified pigment solution. The slight decrease in absorbance is presumably due to pigment degradation caused by the addition of ethanol as the solvent for the retinal. A similar effect was observed after the addition of a similar amount of pure ethanol. Trace d is the difference spectrum between the solution incubated for

[2] The FTIR-difference spectrum of 13-demethylrhodopsin further corroborates this assignment. By analogy with that of 11-*cis*-retinal, the 989 cm^{-1} line is expected to be enhanced in the IR relative to the line at 975 cm^{-1} (Curry, 1983). Consistent with this prediction, the FTIR-difference spectrum of 13-demethylrhodopsin and its metarhodopsin I intermediate shows a negative peak at 988 cm^{-1} but no negative peak at 975 cm^{-1} assignable to the rhodopsin form (Ganter et al., 1990). The absence of a difference band at 975 cm^{-1} could also be due to the fact that the $C_7=C_8$ region of the chromophore is largely unaffected by the isomerization, since this mode is further removed from the Schiff base terminus of the chromophore. Both explanations support our assignment. In addition, the observation of a downshift of the 989 cm^{-1} mode to 980 cm^{-1} in D_2O suggests that this mode is located closer to the PSB terminus of the chromophore (Ganter et al., 1990).

24 h and the solution incubated for 10 min. This difference spectrum shows only a very slight decrease in absorbance, suggesting that the extinction coefficient of 10-methyl-13-demethylrhodopsin is slightly higher than that of rhodopsin. To quantify this difference, the extent of chromophore exchange must be determined.

The spectrum of the solution after incubation with a 10-fold molar excess of 11-*cis*-retinal for 10 min followed by bleaching with NH_2OH for 24 h is displayed in trace e. There is an almost complete bleach of the absorbance at 500 nm, consistent with the absence of rhodopsin after this short incubation time. The spectrum of the NH_2OH-bleached solution of 10-methyl-13-demethylrhodopsin incubated with 11-*cis*-retinal for 24 h is presented in trace f. For better display, spectrum e has been subtracted from this spectrum to remove background due to retinal oxime. The strong residual absorbance at 500 nm clearly demonstrates that chromophore exchange did take place, forming NH_2OH-stable rhodopsin. Comparison of this spectrum with the original absorption spectrum shows that approximately 50% of the analog protein molecules have exchanged their chromophore for 11-*cis*-retinal. The 3% decrease in absorption in trace d upon exchange of 50% of the chromophores suggests that the extinction coefficient of 10-methyl-13-demethylrhodopsin is approximately 6% higher than the extinction coefficient of rhodopsin. The extinction coefficient of rhodopsin in CHAPSO is ~38000 M^{-1} cm^{-1} (Gaertner et al., 1991). The extinction coefficient of 10-methyl-13-demethylrhodopsin in buffer A is therefore 40 000 ± 5000 M^{-1} cm^{-1}. Our error estimate reflects uncertainty in the rhodopsin extinction coefficient and experimental uncertainty in the determination of a small change in absorbance in the presence of a large scattering background in our experiment.

We performed an analogous experiment with 13-demethylrhodopsin. Since this pigment is more stable, we only achieved ~30% exchange in the 24 h exchange period, resulting in a decrease in absorbance of about 2%. The extinction coefficient of 13-demethylrhodopsin in buffer A is therefore 40 000 ± 5000 M^{-1} cm^{-1}. Our extinction coefficient of 13-demethylrhodopsin in buffer A is in good agreement with the previously published result (38 000 M^{-1} cm^{-1}; Nelson et al., 1970).

Since the quantum yield experiments were conducted in Ammonyx/HPO_4^{2-} with 2 mM CHAPSO, we had to determine the change in extinction coefficient for the transfer of the analogs from buffer A to Ammonyx/HPO_4^{2-}. The observed 6% increase in extinction for the transfer of rhodopsin from buffer A into Ammonyx/HPO_4^{2-} (Figure 2) is consistent with the published extinction coefficients of rhodopsin in CHAPSO (ϵ = 38 000 M^{-1} cm^{-1}; Gaertner et al., 1991) and Ammonyx (ϵ = 40 600 M^{-1} cm^{-1}; Wald & Brown, 1954). We observe a 10% extinction coefficient increase for 13-demethylrhodopsin and 10-methyl-13-demethylrhodopsin in Ammonyx compared to buffer A. The extinction coefficient in Ammonyx is therefore 44 000 ± 5000 M^{-1} cm^{-1} for 13-demethylrhodopsin and 44 000 ± 5000 M^{-1} cm^{-1} for 10-methyl-13-demethylrhodopsin.

Quantum Yield Experiments. In quantum yield experiments, it is important that the photoproducts such as metarhodopsin I do not absorb at the probing wavelength. In Ammonyx/HPO_4^{2-}, all the photoproducts denature, resulting in a unique absorption maximum at 380 nm. Figure 7 displays the absorption spectra of rhodopsin (A), 13-demethylrhodopsin (B), and 10-methyl-13-demethylrhodopsin (C) in Ammonyx and the spectra of the proteins after partial and total bleaching. The isosbestic point observed in these spectra demonstrates that under these conditions only two species are formed. The spectra of the bleached pigments also demonstrate that the photoproduct does not exhibit any absorbance at the probing wavelengths under our experimental conditions.

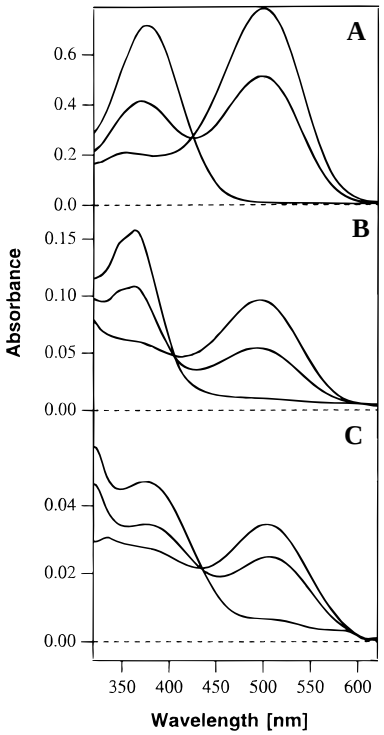

FIGURE 7: Visible absorption spectra of rhodopsin (A), 13-demethylrhodopsin (B), and 10-methyl-13-demethylrhodopsin (C) in 30 mM HPO_4^{2-} and 3% Ammonyx. As the visible absorption decreases due to photolysis, a new band at 380 nm emerges.

A representative set of absorption decay traces is displayed in Figure 8. The decay at a 2 nm bandwidth is displayed in the upper trace (open diamonds), while the decay at a 12 nm bandwidth is displayed in the lower trace (filled diamonds). The curves displayed have been fit with a linear regression with R values better than 0.99. The decay rate at a 2 nm bandwidth was subtracted from the decay rate at a 12 nm bandwidth to yield the pure photobleaching rate. The photobleaching rates were averaged over four measurements. The average decay rate ratio ρ was 0.77 ± 0.1 for 13-demethylrhodopsin and 0.57 ± 0.14 for 10-methyl-13-demethylrhodopsin. As a control experiment, we also measured the decay rate of isorhodopsin. We obtained a ρ of 0.37 ± 0.05. From these ratios, we determined the reaction quantum yield of the respective analog pigments using values of 40 600 M^{-1} cm^{-1} for the extinction coefficient and 0.67 for the reaction quantum yield of rhodopsin (Dartnall et al., 1936; Wald & Brown, 1954), 43 000 M^{-1} cm^{-1} for the extinction coefficient of isorhodopsin (Wald & Brown, 1954), and 44 000 M^{-1} cm^{-1} for the extinction coefficients of 13-demethylrhodopsin and 10-methyl-13-demethylrhodopsin. Since the absorption spectral shape for rhodopsin and the three analogs is nearly identical, these numbers can be used in eq 5 to analyze the absorption decay at any wavelength. Equation 5 yields an isomerization quantum yield of 0.47 ± 0.09 for 13-demethylrhodopsin and 0.35 ± 0.07 for 10-methyl-13-demethylrhodopsin. The quantum yield of isorhodopsin is found to be 0.25 ± 0.04,

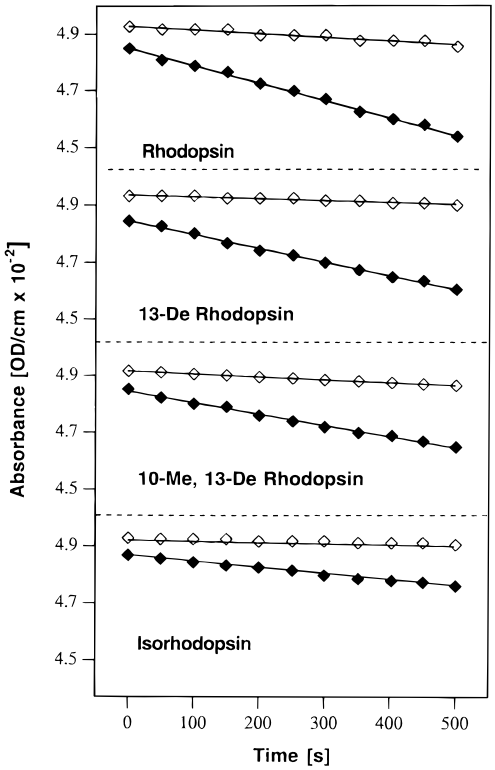

FIGURE 8: Photobleaching decay curves for rhodopsin, 13-demethylrhodopsin, and 10-methyl-13-demethylrhodopsin at 530 nm and isorhodopsin at 514 nm. The decay was first measured at a 2 nm bandwidth (◇). The excitation bandwidth was then increased to 12 nm and the decay measured under these conditions (◆). The traces are normalized to an initial optical density of 0.05 OD/cm.

Table 1: Rhodopsin Photoproduct Formation Times and Quantum Yields

analog chromophore	reaction quantum yield	photoproduct formation time (fs)
11-*cis*-retinal	0.67[d]	200[a]
13-demethyl 11-*cis*-retinal	0.47	400[b]
9-*cis*-retinal	0.25[e]	600[c]
10-methyl-13-demethyl-11-*cis*-retinal	0.35	nd[f]

[a] Peteanu et al. (1993) and Schoenlein et al. (1991). [b] Wang et al. (1996). [c] Schoenlein et al. (1993). [d] Wald (1968). [e] Hurley et al. (1977) and Liu et al. (1986). [f] nd, not determined.

in good agreement with previously published results (Hurley et al., 1977; Liu et al., 1986). The results of the quantum yield experiments are summarized in Table 1.

DISCUSSION

Isomerization Quantum Yield of Pigment Analogs. The absorption maximum and extinction coefficient of 13-demethylrhodopsin ($\lambda_{max} = 500$ nm, $\epsilon = 44\,000$ M^{-1} cm^{-1}) and its CD spectrum agree within the error with previously published data (Lin, 1994; Nelson et al., 1970; Randall et al., 1991). The 500 nm absorption maximum of 10-methyl-13-demethylrhodopsin suggests that the chromophore is bound to the rhodopsin retinal binding site and not to membrane lipids and/or nonspecific lysine residues. The absence of any significant changes in the absorption maxima of these rhodopsin analogs demonstrates that all the dominant protein−chromophore interactions that control the absorption maximum of rhodopsin are maintained in the analogs, presumably due to the constraining shape of the chromophore binding site.

However, the slow formation rate and thermal lability of the 10-methyl-13-demethyl pigment suggest that it does not perfectly fit into the rhodopsin binding site. The exchange of both chromophores with 11-*cis*-retinal demonstrates that they compete for the same binding site as 11-*cis*-retinal. Our value for the quantum yield of 13-demethylrhodopsin of 0.47 is almost twice as large as the previously determined value of 0.24 (Nelson et al., 1970). However, the sample used in the previous study was studied in the nondenaturing detergent digitonin. In nondenaturing detergents, 13-demethylrhodopsin does not fully bleach but instead forms a mixture of species absorbing at 485 and 380 nm. Since the pigment solution was not purified in the previous study, the steep background due to excess retinal and oxime might have concealed the buildup of intermediates. We prevented the formation of the 485 nm species by conducting our photobleaching rate measurements in the denaturing detergent Ammonyx, in which complete bleaching is achieved. Our higher value for the reaction quantum yield is consistent with the bleach recovery (∼40%) observed in recent femtosecond time-resolved transient absorption experiments (Wang et al., 1996).

Chromophore Distortion in Pigment Analogs. The CD and Raman spectra show that we successfully eliminated the C_{11}═C_{12} distortion in 13-demethylrhodopsin and reintroduced the twist in 10-methyl-13-demethylrhodopsin. In the CD spectrum of rhodopsin, the α-band at 500 nm is believed to be influenced by the distortion of the main polyene chain (Honig et al., 1973; Rafferty et al., 1977; Yoshizawa & Shichida, 1982). The reduction in circular dichroism of the α-band in 13-demethylrhodopsin provides strong evidence for a planarization of the retinal chromophore. The CD spectrum of 13-demethylrhodopsin is also strikingly similar to the CD spectrum of a retinal analog in which C_{11}═C_{12} has been forced to planarity by bridging with a five-membered ring (Fukada et al., 1984). With the reintroduction of the steric interaction in 10-methyl-13-demethylrhodopsin, the α-band grows back in, consistent with the reintroduction of a chromophore twist. The α-band appears even larger for the 10-methyl analog than for rhodopsin, suggesting that there are new chromophore−protein interactions in addition to the nonbonded interaction. The β-band at ∼340 nm is very similar for the three rhodopsins. This suggests that the ionone ring portion of the chromophore is in a similar environment for all three rhodopsins, as the β-band has previously been associated with the distortion of the β-ionone ring of the retinal chromphore (Kropf et al., 1973; Rafferty et al., 1977; Wada et al., 1995). This is supported by the disappearance of circular dichroism upon saturation or epoxide formation on the C_5═C_6 region of the chromophore (Nelson et al., 1970). Additionally, recent CD experiments report a 2-fold increase of this band upon planarization of C_6−C_7 through a methylene bridge (Wada et al., 1995).

The differences in the HOOP region in the resonance Raman spectra of the three rhodopsins provide further information on the structural changes of the chromophore. Torsional double-bond distortion induces intensity in adjacent HOOP modes by lowering the local symmetry and increasing the displacement of the potential well on the excited state surface in this mode (Eyring et al., 1982). The Raman spectrum of rhodopsin displays strong intensity in the HC_{11}═$C_{12}H$ A_2 HOOP mode that has been attributed to chromophore distortions around C_{11}═C_{12} (Eyring et al., 1982). The removal of the 13-CH_3 group in 13-demethyl-

rhodopsin dramatically reduces the HOOP intensity in the band at 989 cm^{-1} assigned to the $HC_{11}=C_{12}H$ A_2 HOOP intensity. This proves that the $C_{11}=C_{12}$ torsional distortion in rhodopsin is due to the 10-H−13-CH_3 interaction and that this torsional distortion causes enhanced HOOP intensities. Addition of the 10-CH_3 group in 10-methyl-13-demethylrhodopsin causes the reappearance of strong HOOP intensity, consistent with the reintroduction of a twist around $C_{11}=C_{12}$.

Further evidence on chromophore structure can be obtained from the Raman intensities in the torsional region. Extensive analysis of low-frequency Raman spectra of isotopically labeled rhodopsins assigned the mode at 569 cm^{-1} to the $C_{11}=C_{12}$ torsion (Lin, 1994). While usually Raman forbidden, this torsion is predicted to gain intensity when $C_{11}=C_{12}$ is distorted. Consistently, after removal of the 13-CH_3 group in 13-demethylrhodopsin, no double-bond torsion with significant intensity is observed in the Raman spectrum. In 10-methyl-13-demethylrhodopsin, the torsional mode reappears with similar intensity as in rhodopsin at 588 cm^{-1}. As discussed above, this mode is either dominantly a $C_{11}=C_{12}$ torsion or a CH_3 wagging combination that has gained intensity through coupling to a $C_{11}=C_{12}$ torsion. These studies suggest that the chromophore in rhodopsin is distorted around $C_{11}=C_{12}$, that this distortion is eliminated after removal of the 13-CH_3 group, and that addition of a CH_3 group at the 10-position reintroduces the chromophore twist as a result of the renewed steric interaction. It should be noted, however, that the electron delocalization in the retinal PSB chromophore of rhodopsin causes a reduction in bond order of the formal double bonds and an increase in bond order of the formal single bonds of the polyene chain (Tavan et al., 1985). We therefore expect that the torsional distortion of the chromophore will not be strictly localized in $C_{11}=C_{12}$ but will be distributed into the adjacent ($C_{10}-C_{11}$ and $C_{12}-C_{13}$) single bonds as well.

Effect of the Chromophore Twist on the Reaction Rate and Quantum Yield. Recent femtosecond time-resolved transient absorption experiments have led to the hypothesis that the efficiency of the rhodopsin isomerization is mechanistically linked to the reaction rate through a dynamic coupling mechanism (Kochendoerfer & Mathies, 1995; Wang et al., 1994). It was further hypothesized that the driving force for the rapid reaction rate was a steric nonbonded interaction between the 13-CH_3 and the 10-H groups in rhodopsin. To test these hypotheses, femtosecond time-resolved absorption experiments were performed on 13-demethylrhodopsin, and it was found that the isomerization rate was slowed by a factor of 2 compared to that of rhodopsin (Wang et al., 1996). The reduced reaction quantum yield of 0.47 for 13-demethylrhodopsin further supports the idea that there is a correlation between reaction rate and quantum yield. Table 1 summarizes the reaction quantum yields and photoproduct formation rates of the rhodopsin analogs tested thus far. These data demonstrate a clear correlation between rapid reaction rates and high reaction efficiencies. This correlation is expected to be valid only for those reactions that are fast enough that the dynamic coupling is dominant.

The low-frequency region of the Raman spectra of rhodopsin and 13-demethylrhodopsin provides an additional indication that the initial excited state torsional dynamics in rhodopsin are more rapid. While the spectrum of rhodopsin shows intensity in the $C_{11}=C_{12}$ torsion at 569 cm^{-1}, no mode of similar intensity is observed in the torsional region of the Raman spectrum of 13-demethylrhodopsin. Similarly, the $HC_{11}=C_{12}H$ A_2 HOOP intensity is significantly reduced in the 13-demethyl pigment. Since Raman intensity is induced by rapid evolution along a particular mode upon excitation, the absence of torsional and HOOP modes with large intensity in 13-demethylrhodopsin demonstrates that 13-demethylrhodopsin does not immediately undergo rapid twisting on the excited state potential surface. This slower departure out of the Franck−Condon region is correlated with a slower overall reaction rate and a lower quantum yield. The reappearance of torsional and HOOP intensity in 10-methyl-13-demethylrhodopsin further demonstrates that the torsional Raman intensity in rhodopsin is due to the nonbonded interaction. Since resonance Raman intensities tell us about initial motion along the torsional degrees of freedom, this directly tells us that the 13-CH_3−10-H interaction drives the initial twisting motion along the $C_{11}=C_{12}$ isomerization coordinate.

In rhodopsin, the rapid departure out of the Franck−Condon region is achieved through a steric interaction between the 13-CH_3 and the 10-H groups that introduces a twist in the ground state structure of the 11-*cis*-retinal chromophore and introduces slope to the excited state surface. The chromophore therefore moves rapidly out of the Franck−Condon region along the reaction coordinate and gains torsional momentum. This rapid evolution is shown by the ultrashort fluorescence lifetime of rhodopsin of ∼50 fs (Doukas et al., 1984; Kochendoerfer & Mathies, 1996). The chromophore then crosses from the excited state potential surface to the ground state potential surface according to a dynamic coupling mechanism that can be described by one-dimensional (Landau, 1932; Zener, 1932) or multidimensional models (Miller & George, 1972). In these mechanisms, the probability of a transition from the excited to the ground state surface and therefore the reaction quantum yield is mechanistically linked to the torsional velocity along the reaction coordinate. The Landau−Zener tunneling probability is given by $P \propto \exp -(\Delta E)^2/2h|\Delta F|v$, where v is the nuclear velocity along the torsional isomerization coordinate in the crossing region. Other important parameters are the slope difference ΔF between the two nonadiabatic surfaces and the energy gap ΔE between the adiabatic surfaces. This formula can qualitatively account for the isomerization times observed in rhodopsin, 13-demethylrhodopsin, and isorhodopsin that are summarized in Table 1, giving further support for a new paradigm for visual pigment photochemistry in which high reaction efficiency is mechanistically linked to rapid initial dynamics and the overall reaction rate.

Distortion of 10-Methyl 13-demethylrhodopsin. Despite the reintroduction of a chromophore twist in 10-methyl-13-demethylrhodopsin, the quantum yield of this analog is lower than that of 13-demethylrhodopsin. This suggests that factors other than the steric twist around its $C_{11}=C_{12}$ dominate its long term reaction dynamics. Interestingly, the HOOP mode at 967 cm^{-1} gains considerable intensity compared to that of PSB upon binding to the protein. This mode is most likely assigned to the $HC_7=C_8H$ A_u HOOP vibration. The strong intensity increase in this mode compared to that of the protonated Schiff base in methanol suggests that protein binding induces additional torsional distortion around $C_7=C_8$. This is supported by the increased CD of the α-band compared to that of rhodopsin. A possible alternative explanation is that this mode increases in intensity due to an altered coupling between the $C_7=C_8$ and $C_{11}=C_{12}$ HOOP

modes upon protein binding. Since intense HOOP modes are an indication of torsional double-bond distortion, it appears that the chromophore in 10-methyl-13-demethylrhodopsin is strongly distorted around C_7═C_8 upon binding to the protein. The strong HC_7═C_8H A_u HOOP intensity in the Raman spectrum of isorhodopsin was interpreted similarly (Mathies et al., 1987). This suggests that the methyl group at C_{10} is interacting unfavorably with an amino acid residue in the rhodopsin binding pocket, causing the distortion around C_7═C_8. Upon excitation, the chromophore is evolving along this coordinate in addition to the rhodopsin reaction coordinate in order to relieve the steric strain. This different trajectory might prevent the chromophore from efficient isomerization.

Implications for the Rhodopsin Binding Site. A comparison of the molecular geometry of the native 11-*cis*-retinal chromophore with that of the 10-methyl-13-demethyl retinal analog can give a possible explanation for the hindered binding of the retinal analog. Roughly, the 11-*cis*-retinal chromophore can be divided into three planes. The first plane comprises C_5═C_6 and the β-ionone ring, the second plane the region between C_7 and the 11-*cis* double bond, and the third plane the Schiff base terminus. The relative orientation of these planes is governed by the torsional angle of C_6−C_7 and the torsional angles around the 11-*cis* double bond. These angles are both estimated to be ∼35°, although their sign is unclear (Eyring et al., 1982). The 10-CH_3 group in 10-methyl-13-demethylrhodopsin is located in the second plane, while the 13-CH_3 group in rhodopsin is in the third plane. Since the second and third plane cannot be coplanar in sterically hindered retinals, the two methyl groups must be pointing in different directions. On the other hand, the 9-*cis*-retinal chromophore of isorhodopsin is not sterically hindered. This makes the second and third planes potentially coplanar. As a result, the 13-methyl group of isorhodopsin is pointing in the same direction as the 10-CH_3 group in 10-methyl-13-demethylrhodopsin. Interestingly, isorhodopsin shows strong protein-induced HOOP intensity at 966 cm^{-1} (Mathies et al., 1987). This mode has previously been assigned to the HC_7═C_8H A_u HOOP vibrations. The very similar orientation of the methyl group in these two analogs and the increase in HOOP intensity with the same normal mode character make it likely that the interaction of their respective 10-CH_3 and 13-CH_3 groups with a protein residue is responsible for their distortion around C_7═C_8. This protein residue could possibly push the second plane toward the first plane. This movement is opposed by the steric interaction between the 5-CH_3 group and the 8-H of retinal, resulting in the distortion around C_7═C_8.

This picture is consistent with the two-dimensional shape of the rhodopsin binding pocket that has been mapped by Liu and co-workers in a series of retinal analog studies (Liu et al., 1984). The binding pocket in the chromophore plane between C_{10} and C_{13} is quite flexible in accommodating retinal analogs such as 11-*cis*-10-methylretinal (Asato et al., 1986) and 11-*cis*-13-ethylretinal and 11-*cis*-13-propylretinal (Nakanishi, 1985). In the case of 13-ethylrhodopsin, the CD spectrum indicated little chromophore perturbation compared to that of rhodopsin (Nakanishi, 1985). However, Liu and co-workers also suggested that there might be some restrictions in this area in the third dimension. This was suggested to explain the extremely poor pigment formation by 10-ethylretinal (Asato et al., 1986) which could be due to the interference with the same protein group interacting with 10-methyl-13-demethylretinal. It will now be very interesting to combine the analog studies with site-directed mutagenesis experiments to identify the residue responsible for the steric interaction.

Implications for the Retinal Conformation and Reaction Trajectory. The isomerization rate in 13-demethylrhodopsin is almost 1 order of magnitude faster than the isomerization rate of the 11-*cis*-retinal PSB in solution (Becker et al., 1985; Kandori et al., 1995). This suggests an important influence of the protein on the reaction dynamics. In solution, the 11-*cis*-retinal PSB is in a thermal equilibrium between the *s-trans* and *s-cis* conformation about C_{12}−C_{13} with each of these conformers having two enantiomeric substates with the CH_3 group above or below the C_9═C_{10} plane (Rowan et al., 1974). Analysis of the resonance Raman spectra of rhodopsin has shown that the chromophore is in the *s-trans* conformation around C_{12}−C_{13} (Callender et al., 1976; Eyring et al., 1980). This leaves the two possible enantiomeric C_{12}−C_{13} *s-trans* conformations in which the 13-CH_3 group is above or below the C_9═C_{10} plane. While retinal solutions do not display circular dichroism, a significant CD signal is observed after protein binding, suggesting that, while in solution both enantiomers exist, only one of them is found in the protein. The protein binding pocket therefore exhibits enantiomeric selectivity.

The presence of an amino acid residue close to the 10-CH_3 group of 10-methyl-13-demethylrhodopsin has important implications for the direction of isomerization of the native 11-*cis*-retinal chromphore. The isomerizing double bond could turn either clockwise or counterclockwise upon photoexcitation. However, for one isomerization direction, the amino acid residue interacting with the 10-CH_3 group of the analog would be reached by the 13-CH_3 group of 11-*cis*-retinal after a less than 35° rotation during the isomerization process. This strongly suggests that this interaction will prevent rhodopsin from isomerizing in this direction, thereby making the isomerization process mandatorily unidirectional. This analysis precludes the possibility of the 13-CH_3 group of 11-*cis*-retinal slipping past the 10-H group upon isomerization, consistent with the ultrafast reaction time of 200 fs. The rhodopsin binding site is therefore able to discriminate against less favorable initial conformations and reaction trajectories via selective "solvation". This may play an important role in producing the efficient rhodopsin isomerization kinetics and quantum yield.

Conclusion. This paper demonstrates the value of combining structural and chemical reaction dynamics studies of analogs to elucidate the relationship between the structure and function of visual pigments. We demonstrate that the nonbonded interaction between the 10-H and the 13-CH_3 group causes a distortion of the native rhodopsin chromophore and introduces a significant gradient in its electronic excited state potential surface along the isomerization coordinate. This increased slope accelerates the overall isomerization rate and allows for a high reaction efficiency according to a dynamic coupling mechanism. This result rationalizes the selection of 11-*cis*-retinal as the chromophore in all visual pigments since the distortion is present only in this retinal isomer. The protein matrix may further facilitate the efficient isomerization of this isomer by selecting ground state conformers that can undergo efficient reaction dynamics. If true, this would be an important example of ground state conformational control in a photochemical reaction. This work provides further support for a new mechanism in visual

pigment photochemistry in which a high reaction quantum yield is caused by a rapid reaction rate according to a dynamic internal conversion mechanism.

ACKNOWLEDGMENT

We thank Steve W. Lin, David S. Wexler, and Judy E. Kim for helpful discussions and Phung Tu for expert assistance with the rhodopsin and analog preparation. We also thank Steve W. Lin for providing the Raman spectrum of 13-demethylrhodopsin.

SUPPORTING INFORMATION AVAILABLE

A more detailed discussion of the assignments of the Raman bands of rhodopsin analogs, the results of our QCFF-PI calculations, and a vibrational frequency correlation diagram for the rhodopsin analogs (11 pages). Ordering information is given on any current masthead page.

REFERENCES

Applebury, M. L., Zuckerman, D. M., Lamola, A. A., & Jovin, T. M. (1974) *Biochemistry 13,* 3448−3458.

Asato, A. E., Denny, M., Matsumoto, H., Mirzadegan, T., Ripka, W. C., Crescitelli, F., & Liu, R. S. H. (1986) *Biochemistry 25,* 7021−7026.

Baasov, T., Friedman, N., & Sheves, M. (1987) *Biochemistry 26,* 3210−3217.

Becker, R. S., Freedman, K., Hutchinson, J. A., & Noe, L. J. (1985) *J. Am. Chem. Soc. 107,* 3942−3944.

Broek, A., Muradin-Szweykowska, M., Courtin, J. M. L., & Lugtenburg, J. (1983) *Recl. Trav. Chim. Pays-Bas 102,* 46−51.

Callender, R. H., Doukas, A., Crouch, R., & Nakanishi, K. (1976) *Biochemistry 15,* 1621−1629.

Curry, B. (1983) Ph.D. Thesis, University of California at Berkeley, Berkeley, CA.

Curry, B., Palings, I., Broek, A. D., Pardoen, J. A., Lugtenburg, J., & Mathies, R. (1985) *Adv. Infrared Raman Spectrosc. 12,* 115−178.

Dartnall, H. J. A., Goodeve, C. T., & Lythgoe, R. J. (1936) *Proc. R. Soc. London, Ser. A 156,* 158−170.

De Grip, W. (1982) *Methods Enzymol. 81,* 197−207.

Deng, H., Huang, L., Callender, R., & Ebrey, T. (1994) *Biophys. J. 66,* 1129−1136.

Doukas, A. G., Junnarkar, M. R., Alfano, R. R., Callender, R. H., Kakitani, T., & Honig, B. (1984) *Proc. Natl. Acad. Sci. U.S.A. 81,* 4790−4794.

Eyring, G., Curry, B., Mathies, R., Fransen, R., Palings, I., & Lugtenburg, J. (1980) *Biochemistry 19,* 2410−2418.

Eyring, G., Curry, B., Broek, A., Lugtenburg, J., & Mathies, R. (1982) *Biochemistry 21,* 384−393.

Fukada, Y., Shichida, Y., Yoshizawa, T., Ito, M., Kodama, A., & Tsukida, K. (1984) *Biochemistry 23,* 5826−5832.

Gaertner, W., Ullrich, D., & Vogt, K. (1991) *Photochem. Photobiol. 54,* 1047−1055.

Ganter, U. M., Gärtner, W., & Siebert, F. (1990) *Eur. Biophys. J. 18,* 295−299.

Honig, B., Kahn, P., & Ebrey, T. G. (1973) *Biochemistry 12,* 1637−1643.

Hurley, J. B., Ebrey, T. G., Honig, B., & Ottolenghi, M. (1977) *Nature 270,* 540−542.

Kandori, H., Katsuta, Y., Ito, M., & Sasabe, H. (1995) *J. Am. Chem. Soc. 117,* 2669−2670.

Kochendoerfer, G. G., & Mathies, R. A. (1995) *Isr. J. Chem. 35,* 211−226.

Kochendoerfer, G. G., & Mathies, R. A. (1996) *J. Phys. Chem. 100,* 14526−14532.

Kropf, A., Whittenberger, B. P., Goff, S. P., & Waggoner, A. S. (1973) *Exp. Eye Res. 17,* 591−606.

Landau, L. (1932) *Phys. Z. Sowjetunion 2,* 46.

Lin, S. (1994) Ph.D. Thesis, University of California at Berkeley, Berkeley, CA.

Liu, R., Asato, A. E., Denny, M., & Mead, D. (1984) *J. Am. Chem. Soc. 106,* 8298−8300.

Liu, R. S. H., Crescitelli, F., Denny, M., Matsumoto, H., & Asato, A. E. (1986) *Biochemistry 25,* 7026−7030.

Mathies, R., Oseroff, A. R., & Stryer, L. (1976) *Proc. Natl. Acad. Sci. U.S.A. 73,* 1−5.

Mathies, R. A., Smith, S. O., & Palings, I. (1987) in *Biological Applications of Raman Spectroscopy: Volume 2 - Resonance Raman Spectra of Polyenes and Aromatics* (Spiro, T. G., Ed.) pp 59−108, John Wiley and Sons, Inc., New York.

Miller, W. H., & George, T. F. (1972) *J. Chem. Phys. 56,* 5637−5652.

Nakanishi, K. (1985) *Pure Appl. Chem. 57,* 769−776.

Nelson, R., deRiel, J. K., & Kropf, A. (1970) *Proc. Natl. Acad. Sci. U.S.A. 66,* 531−538.

Oseroff, A. R., & Callender, R. H. (1974) *Biochemistry 13,* 4243−4248.

Palings, I., Pardoen, J. A., van den Berg, E., Winkel, C., Lugtenburg, J., & Mathies, R. A. (1987) *Biochemistry 26,* 2544−2556.

Palings, I., van den Berg, E. M. M., Lugtenburg, J., & Mathies, R. A. (1989) *Biochemistry 28,* 1498−1507.

Peteanu, L. A., Schoenlein, R. W., Wang, Q., Mathies, R. A., & Shank, C. V. (1993) *Proc. Natl. Acad. Sci. U.S.A. 90,* 11762−11766.

Pouchert, C. J. (1989) *The Aldrich library of FT-IR spectra,* Aldrich Chemical Co., Milwaukee, WI.

Rafferty, C. N., Cassim, J. Y., & McConnell, D. G. (1977) *Biophys. Struct. Mech. 2,* 277−320.

Randall, C. E., Lewis, J. W., Hug, S. J., Bjoerling, S. C., Eisner-Shanas, I., Friedman, N., Ottolenghi, M., Sheves, M., & Kliger, D. S. (1991) *J. Am. Chem. Soc. 113,* 3473−3485.

Rowan, R., Warshel, R., Sykes, B., & Karplus, M. (1974) *Biochemistry 13,* 970.

Schoenlein, R. W., Peteanu, L. A., Mathies, R. A., & Shank, C. V. (1991) *Science 254,* 412−415.

Schoenlein, R. W., Peteanu, L. A., Wang, Q., Mathies, R. A., & Shank, C. V. (1993) *J. Phys. Chem. 97,* 12087−12092.

Stryer, L. (1991) *J. Biol. Chem. 266,* 10711−10714.

Tavan, P., Schulten, K., & Oesterhelt, D. (1985) *Biophys. J. 47,* 415−430.

Wada, A., Tsutsumi, M., Inatomi, Y., Imai, H., Shichida, Y., & Ito, M. (1995) *Chem. Pharm. Bull. 43,* 1419−1421.

Wald, G. (1968) *Science 162,* 230−239.

Wald, G., & Brown, P. (1953) *J. Gen. Physiol. 37,* 189−200.

Wang, Q., Schoenlein, R. W., Peteanu, L. A., Mathies, R. A., & Shank, C. V. (1994) *Science 266,* 422−424.

Wang, Q., Kochendoerfer, G. G., Schoenlein, R. W., Verdegem, P. J. E., Lugtenburg, J., Mathies, R. A., & Shank, C. V. (1996) *J. Phys. Chem. 100,* 17388−17394.

Warshel, A. (1973) *Isr. J. Chem. 11,* 709−717.

Warshel, A., & Karplus, M. (1974) *J. Am. Chem. Soc. 96,* 5677−5689.

Yoshizawa, T., & Wald, G. (1967) *Nature 214,* 566−572.

Yoshizawa, T., & Shichida, Y. (1982) *Methods Enzymol. 81,* 634−641.

Zener, C. (1932) *Proc. R. Soc. London, Ser. A 137,* 696−702.

BI961951L